

Seasonal and Interannual Variability of Atmospheric Heat Sources and Moisture Sinks as Determined from NCEP–NCAR Reanalysis

MICHIO YANAI AND TOMOHIKO TOMITA*

Department of Atmospheric Sciences, University of California, Los Angeles, Los Angeles, California

(Manuscript received 2 January 1997, in final form 20 June 1997)

ABSTRACT

Using the National Centers for Environmental Predictions (NCEP)–National Center for Atmospheric Research (NCAR) reanalysis, distributions of the heat source Q_1 and moisture sink Q_2 between 50°N and 50°S are determined for a 15-yr period from 1980 to 1994. Heating mechanisms operating in various parts of the world are examined by comparing the horizontal distributions of the vertically integrated heat source $\langle Q_1 \rangle$ with those of the vertically integrated moisture sink $\langle Q_2 \rangle$ and outgoing longwave radiation (OLR) flux and by comparing the vertical distributions of Q_1 with those of Q_2 .

In northern winter, the major heat sources are located (i) in a broad zone connecting the tropical Indian Ocean, Indonesia, and the South Pacific convergence zone (SPCZ); (ii) over the Congo and Amazon Basins; and (iii) off the east coasts of Asia and North America. In northern summer, the major heat sources are over (i) the Bay of Bengal coast, (ii) the western tropical Pacific, and (iii) Central America. Throughout the year, the South Indian Ocean, eastern parts of the North and South Pacific Oceans, and eastern parts of the North and South Atlantic Oceans remain to be heat sinks. The desert regions such as the Sahara are characterized by large sensible heating near the surface and intense radiative cooling aloft. Over the tropical oceans, heat released by condensation with deep cumulus convection provides the major heat source. The radiative cooling and moistening due to evaporation are dominant features over the subtropical oceans where subsidence prevails. Over the Tibetan Plateau, the profiles of Q_1 and Q_2 show the importance of sensible heating in spring and contributions from the release of latent heat of condensation in summer. Off the east coast of Japan, intense sensible and latent heat fluxes heat and moisten the lower troposphere during winter.

Heat sources in various regions exhibit strong interannual variability. A long (4–5 yr) periodicity corresponding to the variations in OLR and sea surface temperature (SST) is dominant in the equatorial eastern and central Pacific Ocean, while a shorter-period oscillation is superimposed upon the long-period variation over the equatorial Indian Ocean. The interannual variations of $\langle Q_1 \rangle$, OLR, and SST are strongly coupled in the eastern and central equatorial Pacific. However, the coupling between the interannual variations of $\langle Q_1 \rangle$ and OLR with those of SST is weak in the equatorial western Pacific and Indian Ocean, suggesting that factors other than the local SST are also at work in controlling the variations of atmospheric convection in these regions.

1. Introduction

Since the First Global Atmosphere Research Program (GARP) Global Experiment (FGGE) (December 1978–November 1979), many attempts have been made to determine global distributions of atmospheric heat sources and sinks. Wei et al. (1983), Johnson et al. (1987), and Schaack et al. (1990) estimated the seasonal global distributions of the mean tropospheric heating rate through vertical integration of the isentropic mass continuity equation using the National Meteorological

Center [NMC; currently the National Centers for Environmental Prediction (NCEP)] FGGE III-a and European Centre for Medium-Range Weather Forecasts (ECMWF) FGGE III-b analyses. They showed that the major heat sources are located over South America, equatorial Africa, the intertropical convergence zone (ITCZ), the Asian monsoon region, and the oceanic cyclone tracks of the Northern Hemisphere. They also showed that the primary centers of heating migrate meridionally and zonally with the annual variations of the latitude of maximum incoming solar radiation and the planetary-scale land–sea thermal contrast. Schaack et al. (1990) also examined the vertical profiles of the monthly mean heating rates for various geographical regions.

Hoskins et al. (1989) estimated the global-scale atmospheric heat sources and sinks based on the initialized ECMWF–World Meteorological Organization (WMO) analyses from 1979 to 1989. They showed large seasonal and interannual variability of atmospheric heat-

* Current affiliation: International Pacific Research Center, University of Hawaii at Manoa, Honolulu, Hawaii.

Corresponding author address: Dr. Michio Yanai, Department of Atmospheric Sciences, University of California, Los Angeles, 405 Hilgard Avenue, Los Angeles, CA, 90095-1565.
E-mail: yanai@atmos.ucla.edu

ing during these years. Christy (1991), using the ECMWF analyses from May 1985 to December 1987, calculated vertically integrated diabatic heating rates as residuals of the thermodynamic budget. Trenberth and Solomon (1994) discussed the global heat balance using the top-of-the-atmosphere radiation from the Earth Radiation Budget Experiment with the ECMWF data for each month of 1988. Schaack and Johnson (1994), utilizing the uninitialized ECMWF Tropical Oceans Global Atmosphere (TOGA) analyses, estimated three-dimensional global distributions of atmospheric heating for January and July of the 3-yr period 1986–88, a period that included an El Niño–Southern Oscillation (ENSO) cycle. Their results show that large fluctuations in the magnitude of heating and the disposition of maxima/minima in the Tropics occurred over the 3-yr period. The vertical distributions of heating rate for selected regions also revealed large interannual variability.

On a regional scale, many authors have studied the heat sources and moisture sinks as residuals of the heat and moisture budgets over the Tibetan Plateau and surrounding areas using FGGE II-b and the Chinese Qinghai-Xizang Plateau Meteorology Experiment (QXPME) data (e.g., Nitta 1983; Luo and Yanai 1984; He et al. 1987; Yanai et al. 1992; Yanai and Li 1994a). Their results showed that the time evolution of the Asian summer monsoon is closely related to the horizontal and vertical distributions of atmospheric heating over the Tibetan Plateau and its vicinity. Li and Yanai (1996) showed that the onset of the Asian summer monsoon is concurrent with the reversal of the meridional temperature gradient south of the Tibetan Plateau resulting from the warming of the air above the Eurasian continent centered on the Plateau.

Li and Yanai (1996) also examined the global distributions of heat source and moisture sink of the troposphere using the ECMWF TOGA analyses from 1985 to 1992. They found that strong Asian summer monsoons, as defined by Webster and Yang (1992), are associated with enhanced heating over the Arabian Sea, the Bay of Bengal, and the western Pacific Ocean, and reduced heating over the equatorial Indian Ocean and the central and eastern Pacific. In the year of a weak Asian summer monsoon, the heating over South Asia is significantly weakened, while heating over the equatorial central Pacific to the coast of South America is remarkably enhanced.

As discussed by several authors (e.g., Trenberth and Olson 1988; Hoskins et al. 1989; Schaack and Johnson 1994), however, the continuity of the ECMWF analyses may have been affected by the changes routinely made to the assimilation system for the purpose of improving numerical weather prediction. During the period from 1985 to 1992, several changes in the ECMWF analysis–forecast scheme were made (e.g., Trenberth 1992). The changes in the scheme made during this period may have impact on the analyses and consequently the derived fields such as vertical motion, heating, and drying

rates. Although Yanai and Li (1996) did not find discontinuities in the time series of these quantities during this period, the impact of these changes on the analyses is difficult to ascertain.

Recently, NCEP and the National Center for Atmospheric Research (NCAR) released the global analyses from 1980 to 1994 as part of their 40-yr reanalysis project. The NCEP–NCAR reanalysis uses a frozen global data assimilation system and a database as complete as possible (Kalnay et al. 1996).

The purpose of this paper is to revise and extend the results of Li and Yanai (1996) using the NCEP–NCAR reanalysis from 1980 to 1994. We examine in detail the seasonal and interannual variability of heat sources and moisture sinks and the mechanisms of heating over various geographical regions. In section 2 we discuss the data and analysis procedures of the current work. Section 3 describes the horizontal distributions and seasonal variations of the vertically integrated heat sources and moisture sinks. In section 4 we examine the vertical profiles of heat sources and moisture sinks for various geographical regions to identify the regional characteristics of heating mechanism. Section 5 illustrates interannual variations in heat sources and moisture sinks over four oceanic sectors of the equatorial belt; the equatorial eastern, central, and western Pacific Ocean, and the equatorial Indian Ocean. Regional differences in the degree of coupling between the interannual variations of atmospheric heating, convective activity, and sea surface temperature (SST) are noted. The summary and discussions are given in section 6.

2. Data and analysis procedures

The major data used in this work are the NCEP–NCAR reanalysis on a $2.5^\circ \times 2.5^\circ$ grid for the domain $50^\circ\text{S}–50^\circ\text{N}$; $0^\circ–360^\circ$ from 1980 to 1994. Zonal and meridional wind components and temperature are given at 17 standard pressure levels (1000, 925, 850, 700, 600, 500, 400, 300, 250, 200, 150, 100, 70, 50, 30, 20, and 10 hPa). Relative humidity is given at 8 levels from 1000 to 300 hPa. The NCEP–NCAR reanalysis also provides pressure and other variables at the surface and the tropopause. The global monthly mean outgoing longwave radiation (OLR) flux data edited by the National Oceanic and Atmospheric Administration and the global monthly mean SST data compiled by the United Kingdom Meteorological Office are also used in this work.

The *apparent heat source* Q_1 and the *apparent moisture sink* Q_2 (e.g., Yanai et al. 1973; Yanai and Johnson 1993) are computed from

$$Q_1 = C_p \left(\frac{p}{p_0} \right)^\kappa \left(\frac{\partial \theta}{\partial t} + \mathbf{V} \cdot \nabla \theta + \omega \frac{\partial \theta}{\partial p} \right) \quad \text{and} \quad (1)$$

$$Q_2 = -L \left(\frac{\partial q}{\partial t} + \mathbf{V} \cdot \nabla q + \omega \frac{\partial q}{\partial p} \right). \quad (2)$$

In (1) and (2), θ is the potential temperature, q the mixing ratio of water vapor, \mathbf{V} the horizontal velocity, ω the vertical p -velocity, and p the pressure. In the equation $\kappa = R/C_p$, R , and C_p are, respectively, the gas constant and the specific heat at constant pressure of dry air, $p_0 = 1000$ hPa, L is the latent heat of condensation, and ∇ is the isobaric gradient operator.

In this work, the vertical p -velocity ω is recalculated from the horizontal divergence by vertically integrating the continuity equation

$$\frac{1}{a \cos \phi} \left[\frac{\partial u}{\partial \lambda} + \frac{\partial}{\partial \phi} (v \cos \phi) \right] + \frac{\partial \omega}{\partial p} = 0, \quad (3)$$

with the surface boundary condition

$$\omega = \omega_s = -g\rho_s \left(\frac{u_s}{a \cos \phi} \frac{\partial h}{\partial \lambda} + \frac{v_s}{a} \frac{\partial h}{\partial \phi} \right) \text{ at } p = p_s. \quad (4)$$

In (3) and (4), u and v are the zonal and meridional components of the horizontal wind, a the mean earth radius, λ the longitude, ϕ the latitude, g the acceleration of gravity, ρ the air density, and h the terrain height. The suffix s denotes the surface value. The values of smoothed terrain height on a $2.5^\circ \times 2.5^\circ$ mesh are taken from the NCEP global elevation data.

To obtain reliable estimates of Q_1 and Q_2 , we need accurate estimates of ω to be used in (1) and (2). The estimate of the vertical advection term in (1) in the upper troposphere is extremely sensitive to ω because of high static stability. Above the tropopause, where the convective heat transport vanishes, we may set

$$Q_1 = Q_R, \quad (5)$$

where Q_R is the radiative heating rate. Nitta (1977) assumed (5) at $p = p_T$, where p_T is the tropopause pressure. Because of the lack of three-dimensional data of Q_R , we impose the adiabatic condition

$$\omega = \omega_T = - \left(\frac{\partial \theta}{\partial t} + \mathbf{V} \cdot \nabla \theta \right) / \left(\frac{\partial \theta}{\partial p} \right) \quad (5a)$$

at $p = p_T$. This may be an acceptable approximation to (5), because the magnitude of Q_R is generally small near the tropopause (e.g., Dopplack 1979; Ackerman and Cox 1987). The original estimates of the horizontal divergence, D_0 , are adjusted by adding

$$D' = \left(\omega_T - \omega_s - \int_{p_T}^{p_s} D_0 dp \right) / (p_s - p_T). \quad (6)$$

Then the corrected divergence, $D = D_0 + D'$, is used in (3) to obtain the adjusted values of ω at all levels.

The values of Q_1 and Q_2 are calculated for the layer between the ground surface and the first standard pressure level above the surface, for each successive layer between the standard pressure levels, and between the tropopause and the standard pressure level immediately below it. Because of the horizontally varying terrain

height and tropopause pressure, the number of layers for which Q_1 and Q_2 values are obtained may vary from one grid point to the next. To obtain reliable estimates of Q_1 and Q_2 from (1) and (2) using ω obtained from (3), we design the finite-difference forms for the horizontal and vertical advection terms of (1) and (2) to maintain their consistency with the mass continuity equation that is given in a flux form. The advection terms are evaluated twice a day (0000 and 1200 UTC) and the local time change terms are evaluated using the centered difference of θ and q over 24 h.

As discussed by Yanai et al. (1973), Q_1 and Q_2 are the residuals of heat and moisture budgets of the resolvable motion and may be interpreted as

$$Q_1 = Q_R + L(c - e) - \frac{\partial}{\partial p} \overline{s' \omega'} \quad \text{and} \quad (7)$$

$$Q_2 = L(c - e) + L \frac{\partial}{\partial p} \overline{q' \omega'}, \quad (8)$$

where c is the rate of condensation per unit mass of air. The value of e is the rate of reevaporation of cloud water. The equation $s = C_p T + gz$ is the dry static energy. The value of T is the temperature. The prime denotes the deviation from the horizontal average due to unresolved eddies such as cumulus convection and turbulence. The eddy vertical flux terms may have significant contributions to Q_1 and Q_2 in highly convective situations. From (7) and (8) we find

$$Q_1 - Q_2 - Q_R = - \frac{\partial}{\partial p} \overline{(s' + Lq') \omega'}. \quad (9)$$

Equation (9) has been widely used to measure the activity of cumulus convection (e.g., Yanai et al. 1973; Yanai and Johnson 1993).

Integrating (7) and (8) from the tropopause pressure p_T to the surface pressure p_s , we obtain

$$\langle Q_1 \rangle = \langle Q_R \rangle + LP + S \quad \text{and} \quad (10)$$

$$\langle Q_2 \rangle = L(P - E), \quad (11)$$

where

$$\langle \rangle = \frac{1}{g} \int_{p_T}^{p_s} (\) dp. \quad (12)$$

The values of P , S , and E are the precipitation rate, the sensible heat flux, and the evaporation rate, respectively, per unit area at the surface. In the above, we ignored the integration from $p = 0$ to p_T .

Equations (7)–(11) are useful for physically interpreting the budget results. First, the relations (10) and (11), with the distribution of OLR, serve to verify the accuracy and mutual consistency of the estimates of Q_1 and Q_2 . If the heating over a certain area is primarily due to the condensation process, the values of $\langle Q_1 \rangle$ and $\langle Q_2 \rangle$ should be similar to each other and the OLR may have a small value. On the other hand, the presence of strong sensible heat flux or evaporation from the surface

may cause significant difference between the horizontal distributions of $\langle Q_1 \rangle$ and $\langle Q_2 \rangle$ (e.g., Luo and Yanai 1984; Yanai et al. 1992).

Second, the comparison between the vertical distributions of Q_1 and Q_2 serves to find the presence or absence of eddy vertical transport process. If the heating is mainly due to the condensation associated with stratiform clouds, the vertical profiles of Q_1 and Q_2 will be very similar. On the other hand, if the release of latent heat is associated with cumulus convection, the profiles of Q_1 and Q_2 will differ from each other and there will be a separation in the levels of peak values of Q_1 and Q_2 because of the presence of eddy vertical transport process (e.g., Yanai et al. 1973; Thompson et al. 1979). If the heating is due to the supply of sensible heat flux from the dry ground surface, we expect to obtain the heat source that does not accompany the moisture sink. In such a situation, the vertical profiles of Q_1 will be determined by the redistribution process due to turbulence or dry thermal convection.

3. Horizontal distributions of heat sources and moisture sinks

The 15-yr mean horizontal distributions of the vertically integrated heat source $\langle Q_1 \rangle$ and moisture sink $\langle Q_2 \rangle$, and OLR flux for northern winter (December–February) are shown together in Fig. 1. During northern winter, the major heat sources ($\geq 100 \text{ W m}^{-2}$) are found along the North Pacific and North Atlantic storm tracks and over southern Africa, South America, and the broad belt spanning from the South Indian Ocean through the Indonesian maritime continent to the South Pacific convergence zone (SPCZ) (Fig. 1a). Heat sinks are found over the Northern Hemisphere (NH) continents and eastern parts of the subtropical Pacific and Atlantic Oceans. The heat sources in the Tropics are generally accompanied by moisture sink $\langle Q_2 \rangle$ of similar magnitude (Fig. 1b) indicating that the release of latent heat of condensation is the major component of heat sources. On the other hand, the heat sources along the North Pacific storm tracks are accompanied by negative values of $\langle Q_2 \rangle$ in the upstream and positive values of $\langle Q_2 \rangle$ in the downstream, showing the changing character of heat source from sensible heat flux from the warm ocean surface to condensation heating. In the oceanic subtropical latitudes, large negative values of $\langle Q_1 \rangle$ and $\langle Q_2 \rangle$ ($\sim -100 \text{ W m}^{-2}$) are indicative of radiative cooling exceeding sensible and latent heating [see (10)] and evaporation exceeding precipitation [see (11)]. The distributions of large positive $\langle Q_1 \rangle$ and $\langle Q_2 \rangle$ in the Tropics are consistent with the distribution of the OLR flux less than 240 W m^{-2} (Fig. 1c), showing that the heating is associated with deep cumulus convection.

In northern spring (March–May), much of the Asian and North American continents become heat sources (Fig. 2a). The contrast of larger values of $\langle Q_1 \rangle$ with generally smaller values of $\langle Q_2 \rangle$ over the continents

(Fig. 2b) suggests that sensible heat flux from the ground surface is the major component of heat sources over these land masses. We note, however, that North Africa and the Indian subcontinent are still clearly heat sinks. The heat sources along the North Pacific and North Atlantic storm tracks are drastically weakened. The heat sources in the South Indian Ocean and SPCZ are also weakened, and the distributions of $\langle Q_1 \rangle$, $\langle Q_2 \rangle$, and OLR flux (Fig. 2c) in the Tropics is nearly symmetric with respect to the equator. Compared with the other seasons, heating and convection in the Tropics are least vigorous in northern spring.

In northern summer (June–August), the major heat sources in the Tropics are located to the north of the equator (Figs. 3a,b). Both heating and convective activity (Fig. 3c) become most robust. Principal heat sources are located over the region of the Asian summer monsoon centered at the Bay of Bengal coast, the tropical western Pacific, the SPCZ, and Central America. The maximum heating exceeds 300 W m^{-2} over the northern Bay of Bengal, 200 W m^{-2} over the South China Sea, the western Pacific east of the Philippines, and over Central America. Cooling extends over much of the Southern Hemisphere (SH) subtropical latitudes and the northeastern parts of the North Pacific and Atlantic Oceans (Fig. 3a). The horizontal distributions of $\langle Q_2 \rangle$ (Fig. 3b) and OLR flux (Fig. 3c) are similar to those of $\langle Q_1 \rangle$ in the Tropics, indicating that the major component of heat source is latent heat released in cumulus convection. Over land areas in higher latitudes, including North America and the Tibetan Plateau, positive $\langle Q_1 \rangle$ values are generally larger than $\langle Q_2 \rangle$ values, implying that sensible heating from ground surface is significant.

In northern fall (September–November), the major convective rainbelt and heat sources in the Eastern Hemisphere have retreated southward and are centered over the equator (Figs. 4a–c). They become less vigorous than in summer. Much of the Eurasian and North American continents become weak heat sinks. Southern Africa and South America become heat sources due to the release of latent heat in deep cumulus convection as indicated by the small values of OLR ($\leq 240 \text{ W m}^{-2}$). The Pacific ITCZ reaches the northernmost position near 10°N (Fig. 4c).

In summary, the large-scale features of the vertically integrated heat sources and moisture sinks obtained in this study are consistent with each other and with those of the OLR flux and other known features of the global circulation. The horizontal distributions and locations of the maxima/minima are generally consistent with previous estimates for corresponding seasons based on FGGE III-a analyses (Wei et al. 1983), FGGE III-b analyses (Schaack et al. 1990), and ECMWF TOGA analyses (Schaack and Johnson 1994; Li and Yanai 1996).

4. Vertical profiles of heating

To identify the principal factors contributing to the heating or cooling over various parts of the world, we

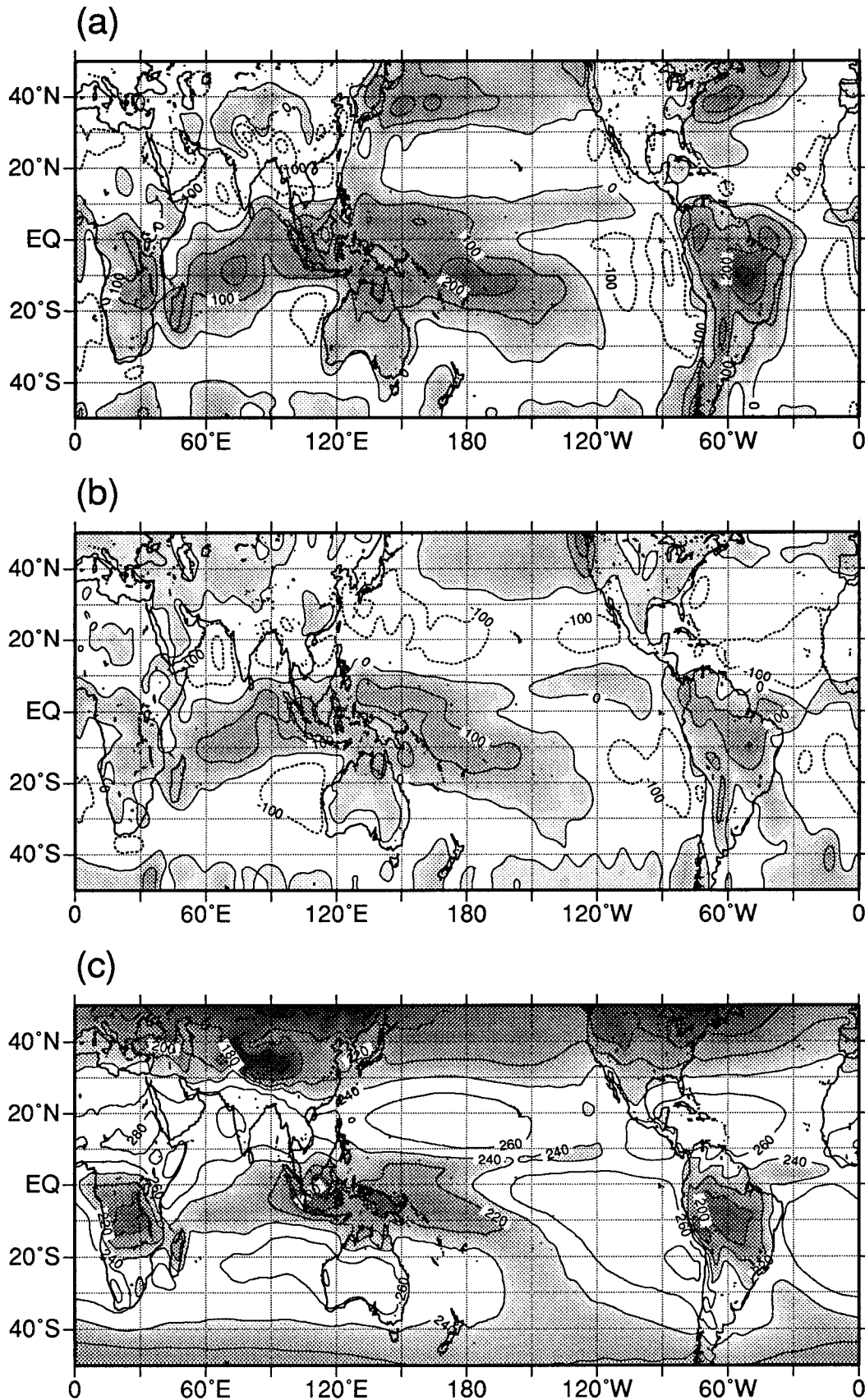


FIG. 1. Global distributions of the 15-yr mean (1980–94) (a) vertically integrated heat source $\langle Q_1 \rangle$; (b) vertically integrated moisture sink $\langle Q_2 \rangle$; and (c) OLR flux (units: W m^{-2}) for northern winter (December–February).

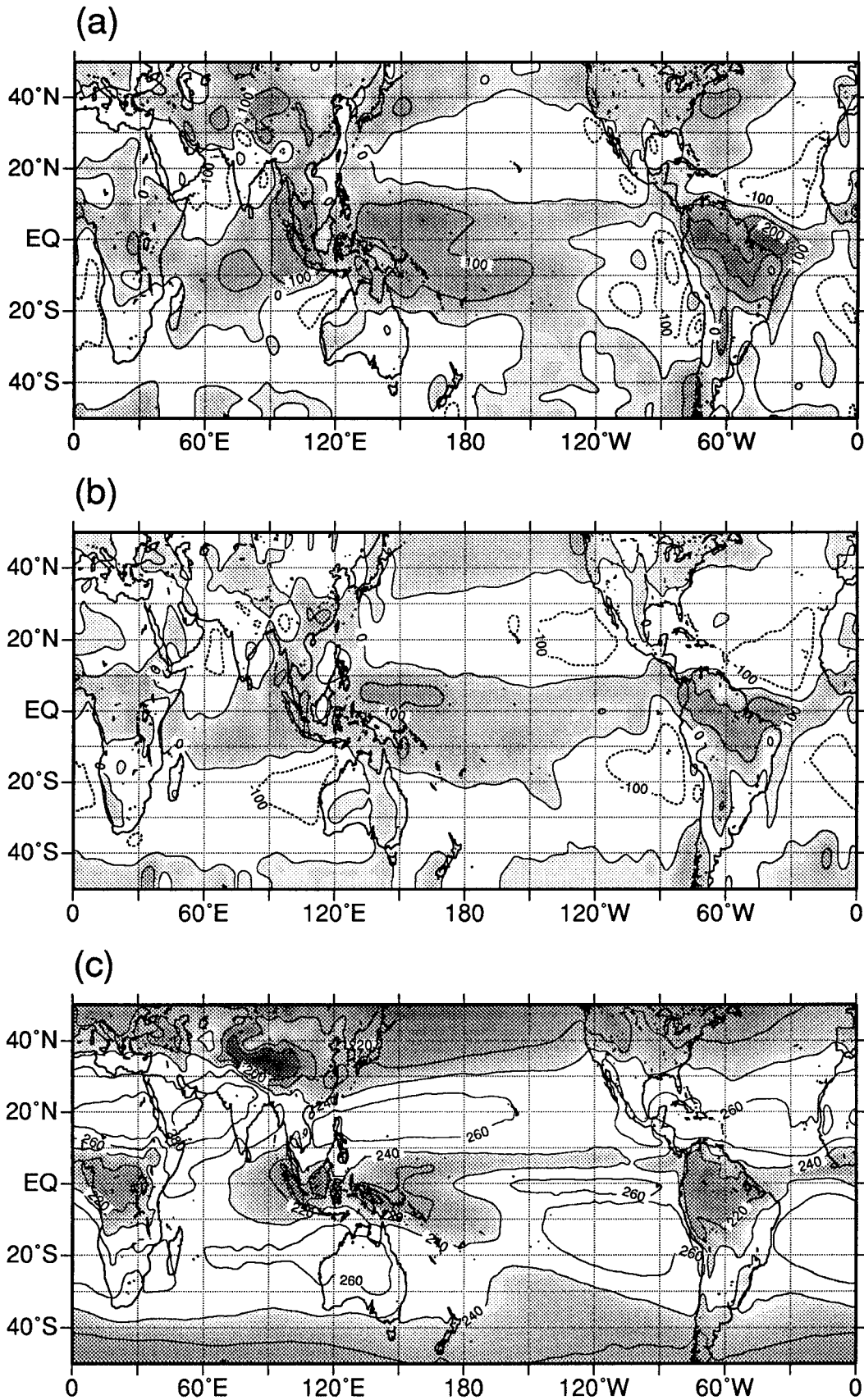


FIG. 2. As in Fig. 1 but for northern spring (March–May).

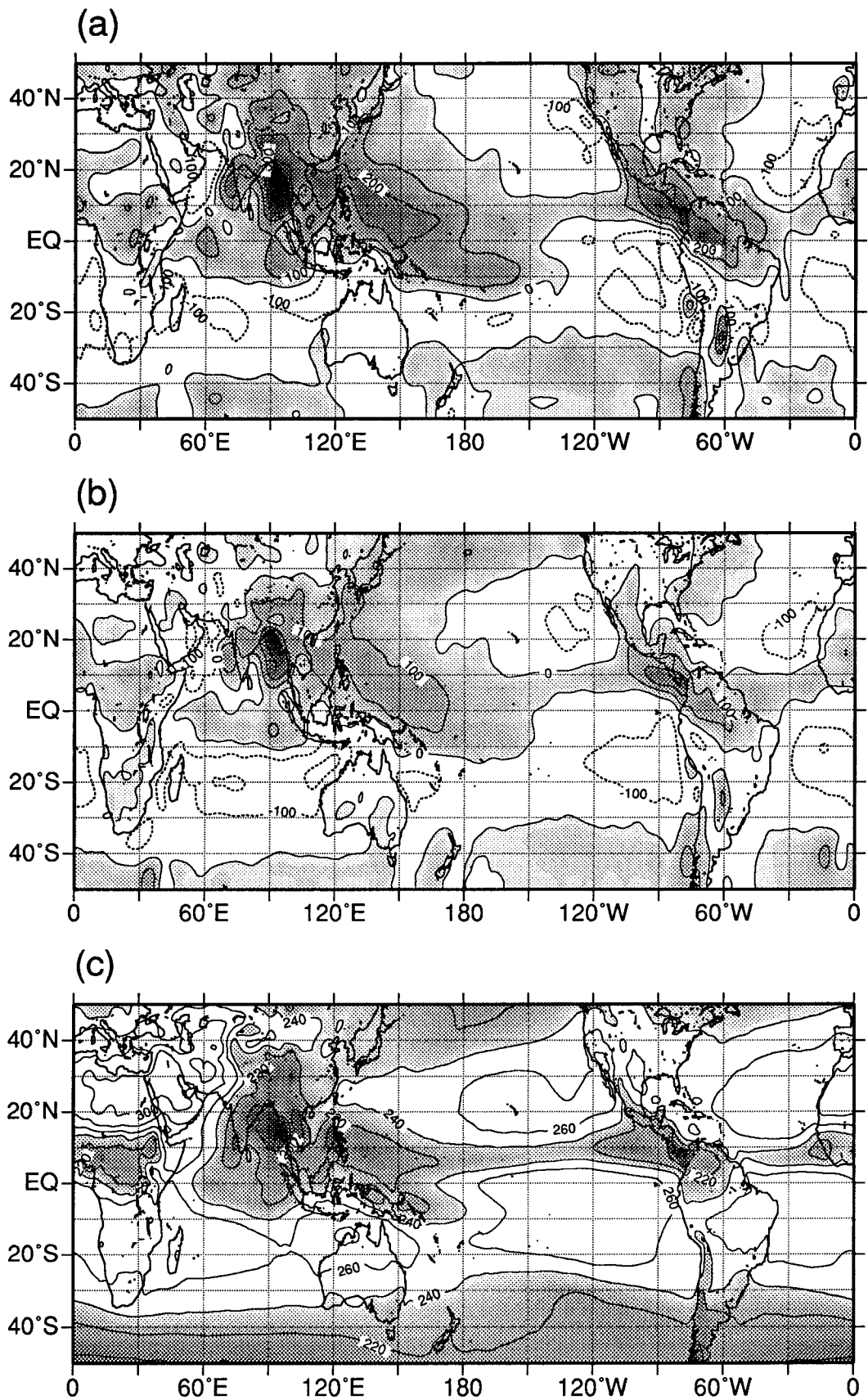


FIG. 3. As in Fig. 1 but for northern summer (June–August).

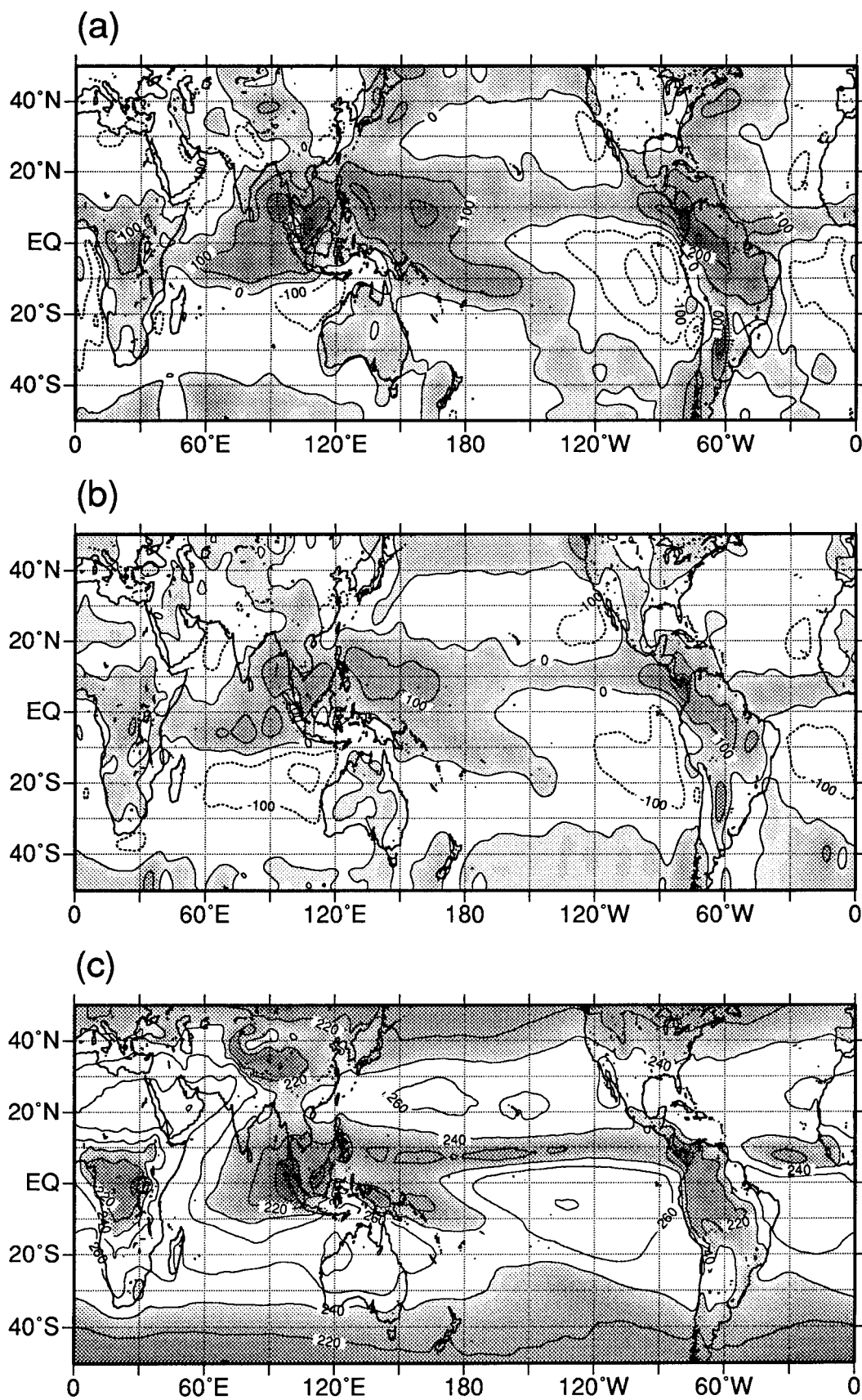


FIG. 4. As in Fig. 1 but for northern fall (September–November).

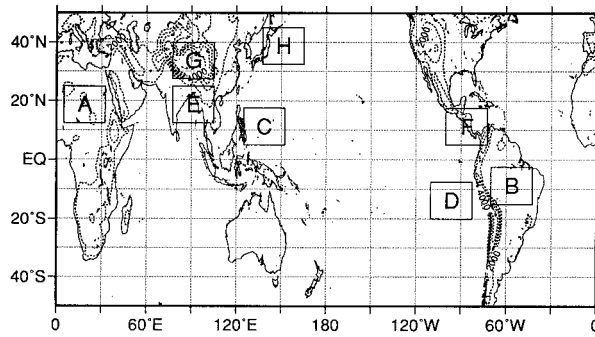


FIG. 5. Regions where the vertical profiles of heat source Q_1 and moisture sink Q_2 are examined.

shall examine the vertical distributions of Q_1 and Q_2 over various regions. Using Figs. 1–4 as a guide, we select eight locations shown in Fig. 5 to study typical regional characteristics of heating and moistening processes. In Figs. 6a–h, we illustrate the mean vertical profiles of Q_1 and Q_2 over these regions for four seasons.

Over the Sahara Desert (Fig. 6a, region A in Fig. 5), the Q_1 values show basically similar vertical distributions throughout the year, that is, positive near the surface and negative in the upper and middle troposphere. The cooling in the upper and middle troposphere is considered to be due to radiation. On the other hand, heating in the lower layer can be explained by the vertical convergence of sensible heat flux from the surface [see (7)]. Throughout the year, Q_2 values are negligibly small in the whole troposphere. In northern summer (June–August), however, Q_2 takes a small positive value near the surface, probably due to the release of latent heat of condensation accompanied by rains. We remark that the vertical profiles of Q_1 and Q_2 over the Australian Desert are very similar to those found over the Sahara (not shown).

The vertical profiles of Q_1 and Q_2 over Brazil (Fig. 6b, region B in Fig. 5) are distinctly different from those over dry land surfaces. In northern winter, spring, and fall, Q_1 and Q_2 values are large positive with separation of peaks in Q_1 (400–600 hPa) and Q_2 (700–850 hPa), indicating the presence of cumulus-convective vertical transport [see (9)]. The heating is strongest in northern winter. During northern summer (dry season in Brazil), the upper troposphere becomes weak heat sink and heating is confined in the lower layers. Schaack et al. (1990) showed similar seasonal variation of the vertical distribution of heating over central Brazil derived from the FGGE III-b analysis.

The vertical profiles of Q_1 and Q_2 over oceans also show a variety of shapes reflecting different heating and moistening processes. The vertical distributions over the western Pacific warm pool (Fig. 6c, region C in Fig. 5), especially those of the northern summer and fall, show large heating centered between 400 and 500 hPa and large drying centered between 600 and 700 hPa. As discussed by Yanai et al. (1973), the vertical separation

of peaks of Q_1 and Q_2 is a characteristic feature associated with cumulus convection [see (9)].

The profiles from the subtropical eastern South Pacific (region D in Fig. 6) are shown in Fig. 6d. In this region, the low-level anticyclonic circulation persists in all four seasons. The radiative cooling and moistening due to evaporation from the surface occur throughout the depth of the troposphere except the layer below 925 hPa, where weak heating appears. Schaack et al. (1990) also obtained similar vertical profiles over the subtropical eastern South Pacific using FGGE III-b analyses. Similar vertical profiles are also obtained over the subtropical eastern North Pacific and the subtropical eastern North and South Atlantic Ocean (not shown).

Figure 6e shows the mean vertical profiles of Q_1 and Q_2 over the region centered on the Bay of Bengal coast (region E in Fig. 5), where large heating associated with the Asian summer monsoon occurs during northern summer (see Fig. 3). In northern winter, Q_1 is negative throughout the troposphere except near the surface; Q_2 is also negative in the lower troposphere. These indicate the dominance of radiative cooling and evaporation before the arrival of monsoon rains (see Fig. 1). In spring, weak heating with condensation appears in the lower troposphere corresponding to the arrival of monsoon rains (see Fig. 2). During northern summer, large positive values of Q_1 and Q_2 occur throughout the troposphere. The magnitudes of Q_1 and Q_2 are similar to each other, but their peaks are separated showing that the heating occurs in association with deep cumulus clouds. The magnitude and vertical distribution of Q_1 are very similar to those obtained by Schaack et al. (1990) using the FGGE III-b analysis. During northern fall, both Q_1 and Q_2 are substantially weakened since the major rainbelt in South Asia begins to retreat southward (see Fig. 4).

The vertical distributions over the Arabian Sea (not shown) during northern winter, spring, and fall are characterized by cooling throughout the troposphere and large negative Q_2 (moistening) in the lower layers. These are consistent with the radiative cooling discussed by Ackerman and Cox (1987) and strong evaporation from the sea surface (e.g., Rao et al. 1981; Mohanty et al. 1983). After the onset of the Indian monsoon in June, southwest India receives rains, but most of the Arabian Sea continues to experience subsidence, radiative cooling, and intense evaporation (e.g., Yanai et al. 1992).

Region F is a mostly oceanic region centered over Central America (see Fig. 5), where heavy rains fall during northern summer and fall with the “Mexican monsoon” (e.g., Douglas et al. 1993). Here, changes in the vertical profiles of Q_1 and Q_2 , similar to those in region E, occur with the progress of the season (Fig. 6f). Reflecting the seasonal migration of the ITCZ, large heating and drying occur during northern summer and fall (see Figs. 3 and 4). The vertical distributions of Q_1 and Q_2 during the rain season clearly show the effect of cumulus convection.

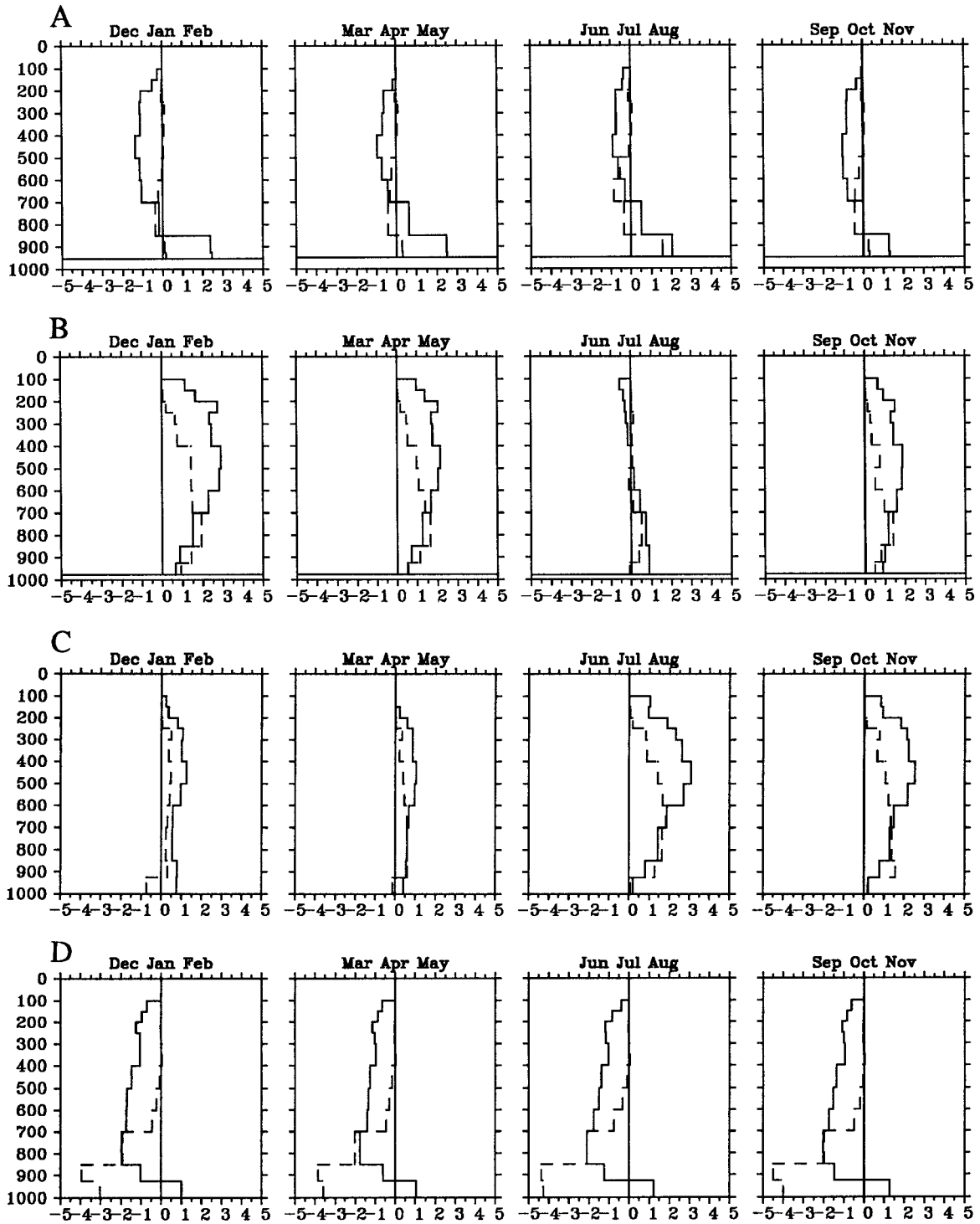


FIG. 6. Seasonal mean vertical profiles of heat source Q_1 and moisture sink Q_2 averaged over various regions shown in Fig. 5. (a) Sahara, (b) Brazil, (c) the western tropical Pacific, (d) the eastern South Pacific, (e) the Bay of Bengal, (f) the oceanic region centered over Panama, (g) the Tibetan Plateau, and (h) off the east coast of Japan.

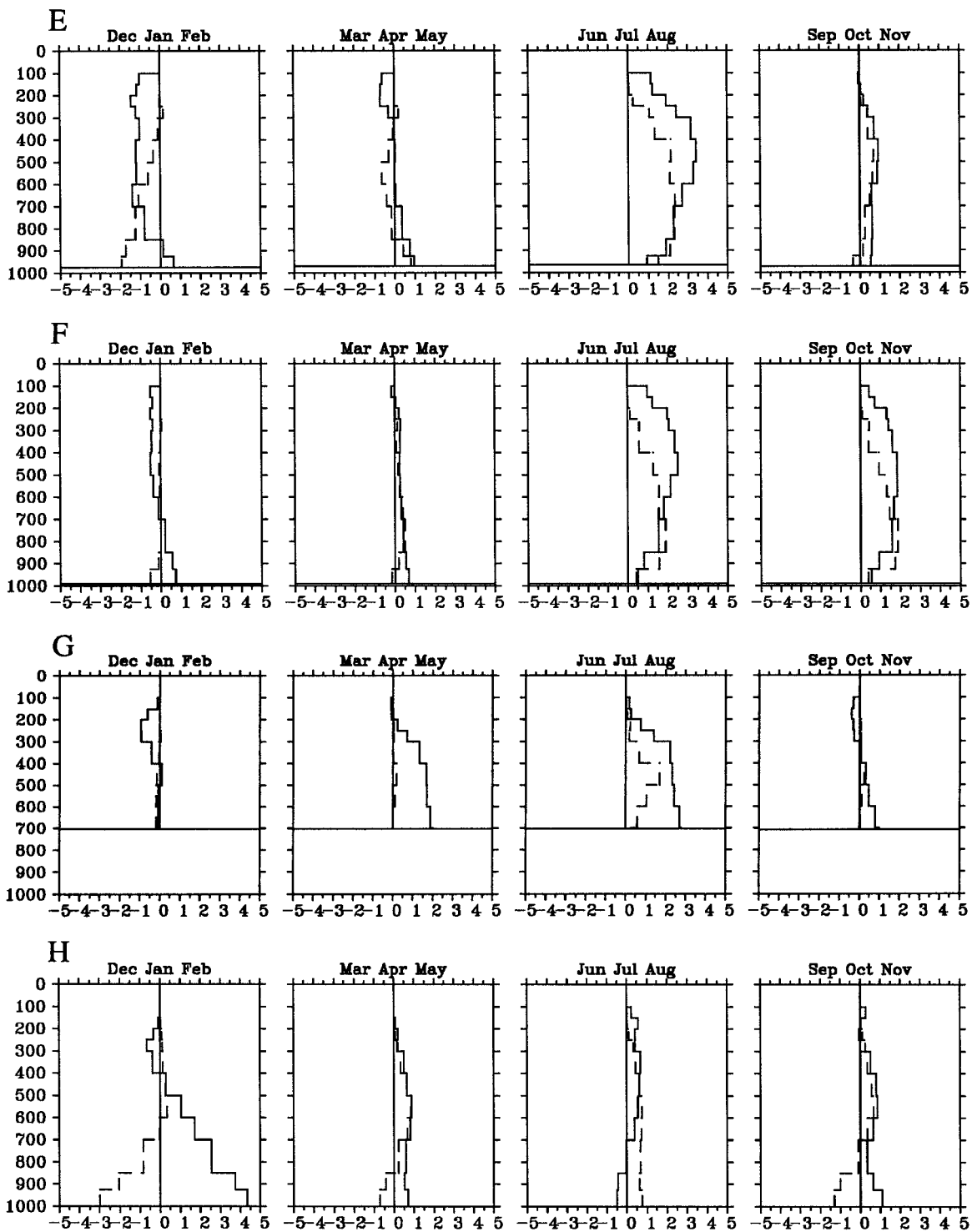


FIG. 6. (Continued)

Figure 6g shows seasonal mean vertical profiles of Q_1 and Q_2 for the Tibetan Plateau. Because of sparse upper-air observations over this region, except during the FGGE year of 1979, the vertical profiles are not discussed separately for the western and eastern parts

of the Plateau as in previous papers (e.g., Luo and Yanai 1984; Yanai et al. 1992; Yanai and Li 1994a). During northern winter, the Q_1 values are negative, suggesting radiative cooling and the Q_2 values are negligibly small. In spring, Q_1 over the Plateau becomes positive through-

out the troposphere, but Q_2 is still very small. These suggest that sensible heating from the Plateau surface is the major mechanism of heating during this season (Luo and Yanai 1984; Yanai and Li 1994a). In northern summer, Q_1 over the Plateau shows intense heating ($2\sim 3$ K day⁻¹) in the layer between 300 hPa and the surface. Here, Q_2 is also positive ($1\sim 2$ K day⁻¹) in this layer, indicating that both sensible heating and condensation heating are contributing to the heat source as previously shown by Nitta (1983), Luo and Yanai (1984), and others. In fall, heating over the Tibetan Plateau is much reduced, and Q_1 is negative above the 300-hPa level indicating radiative cooling. The changing vertical profiles from northern winter to summer are consistent with those of the corresponding seasons obtained by Yanai et al. (1992) using the FGGE II-b data.

We also investigated the vertical profiles of Q_1 and Q_2 over the high Plains region of the western United States (not shown). The vertical profiles and their seasonal changes are similar to those over the western Tibetan Plateau (Yanai et al. 1992). The radiative cooling is dominant in winter, then the sensible heating becomes a major component of heat source in spring. In summer, the sensible heating is still dominant over this region, and Q_2 is negative in the lower layer. In fall, the radiative cooling becomes the dominant process in the upper and middle troposphere.

Finally, Fig. 6h shows the Q_1 and Q_2 profiles for the region east of Japan (region H in Fig. 5). In northern winter, Q_1 is strongly positive in the lower tropospheric layer and decreases with height and becomes negative above 400 hPa. On the contrary, Q_2 is strongly negative near the surface and increases with height and becomes weak positive above the 600-hPa level. The strong low-level heating and moistening suggests intense sensible heat flux and evaporation from the warm ocean surface of the Kuroshio and North Pacific Current. In northern spring, low-level heating and moistening are substantially weakened. During northern summer, Q_1 becomes weak negative, and Q_2 becomes weak positive in lower levels. In fall, the vertical profiles of Q_1 and Q_2 are similar to those in winter except that their magnitudes are smaller. Similar vertical profiles of Q_1 and Q_2 and their seasonal variations are observed off the east coast of North America (not shown).

5. Interannual variability of heat sources

In this section, we examine the interannual variability of heat sources and moisture sinks over the equatorial oceans. The most conspicuous and well-documented interannual timescale in climate variability is that of El Niño–Southern Oscillation (e.g., Philander 1990; Rasmusson and Carpenter 1982). The ENSO events are associated with large SST anomalies and eastward or westward displacement of convective activity in the tropical Pacific Ocean and anomalous monsoon precipitation in South Asia (e.g., Rasmusson and Carpenter 1983; Ro-

pelewski and Halpert 1987, 1989; Krishnamurti et al. 1989, 1990; Joseph et al. 1994). During the analysis period from 1980 to 1994, there were three major ENSO events: 1982–83, 1986–88, and 1991–92.

In the following discussion, the monthly anomalies of $\langle Q_1 \rangle$, $\langle Q_2 \rangle$, OLR, SST, and other variables are obtained by subtracting the average of monthly mean values for the 15 yr (1980–94) from the original monthly mean values of these variables. In order to highlight interannual variability, an 11-term low-pass filtering (Trenberth 1984) is applied to the time series of a monthly anomaly of each variable.

In Figs. 7, 8, 9, and 10, we show time series of the low-pass filtered $\langle Q_1 \rangle$, $\langle Q_2 \rangle$, OLR, SST, and horizontal divergence at 850 and 200 hPa for four oceanic sectors of the equatorial belt (between 5°N and 5°S). These sectors are the eastern, central, and western parts of the equatorial Pacific Ocean and the equatorial Indian Ocean. For all four sectors, $\langle Q_1 \rangle$ and $\langle Q_2 \rangle$ curves are very similar to each other showing that release of latent heat of condensation is the primary heat source over the equatorial oceans.

The magnitudes of $\langle Q_1 \rangle$ and SST anomalies in the eastern equatorial Pacific Ocean show their maxima during the 1982 ENSO event (Fig. 7). The magnitude of interannual variation in $\langle Q_1 \rangle$ generally decreases westward (Figs. 8–10). (Note that the vertical scales for the panels in Figs. 8–10 are different for each sector.) The sign of the $\langle Q_1 \rangle$, OLR, and SST anomalies reverses between the central equatorial Pacific (Fig. 8) and the western equatorial Pacific (Fig. 9). In the equatorial Indian Ocean, the $\langle Q_1 \rangle$, OLR, and SST anomalies are again nearly in phase with those of the eastern and central Pacific Ocean.

There is a systematic change in the dominant periodicity of $\langle Q_1 \rangle$ anomaly from the eastern Pacific Ocean to the Indian Ocean. In the eastern (Fig. 7) and central Pacific Ocean (Fig. 8), a longer ($\sim 4\text{--}5$ yr) periodicity with ENSO is dominant, and this low-frequency variability is remarkably well correlated with similar variability of OLR, SST, and horizontal divergence (out of phase between 850 and 200 hPa). The high correlations with these variables suggest that anomalous heating over these sectors is accompanied by intensified convective activity favored by warmer SST. In the equatorial western Pacific (Fig. 9) and Indian Ocean (Fig. 10), on the other hand, oscillations of $\langle Q_1 \rangle$ with shorter periods ($\sim 1\text{--}2$ yr) are superimposed upon the longer periods ($\sim 5\text{--}6$ yr).

Table 1 shows the correlation coefficients between $\langle Q_1 \rangle$ and OLR, SST, and horizontal divergence at 850 and 200 hPa for the four oceanic sectors. We note that absolute values of the correlation coefficients shown in Table 1 are well over 0.6 except for those with SST in the equatorial western Pacific and Indian Oceans. The interannual variability of $\langle Q_1 \rangle$ over the whole equatorial Pacific Ocean is well related to the interannual variability of convective activity (OLR) and low-level con-

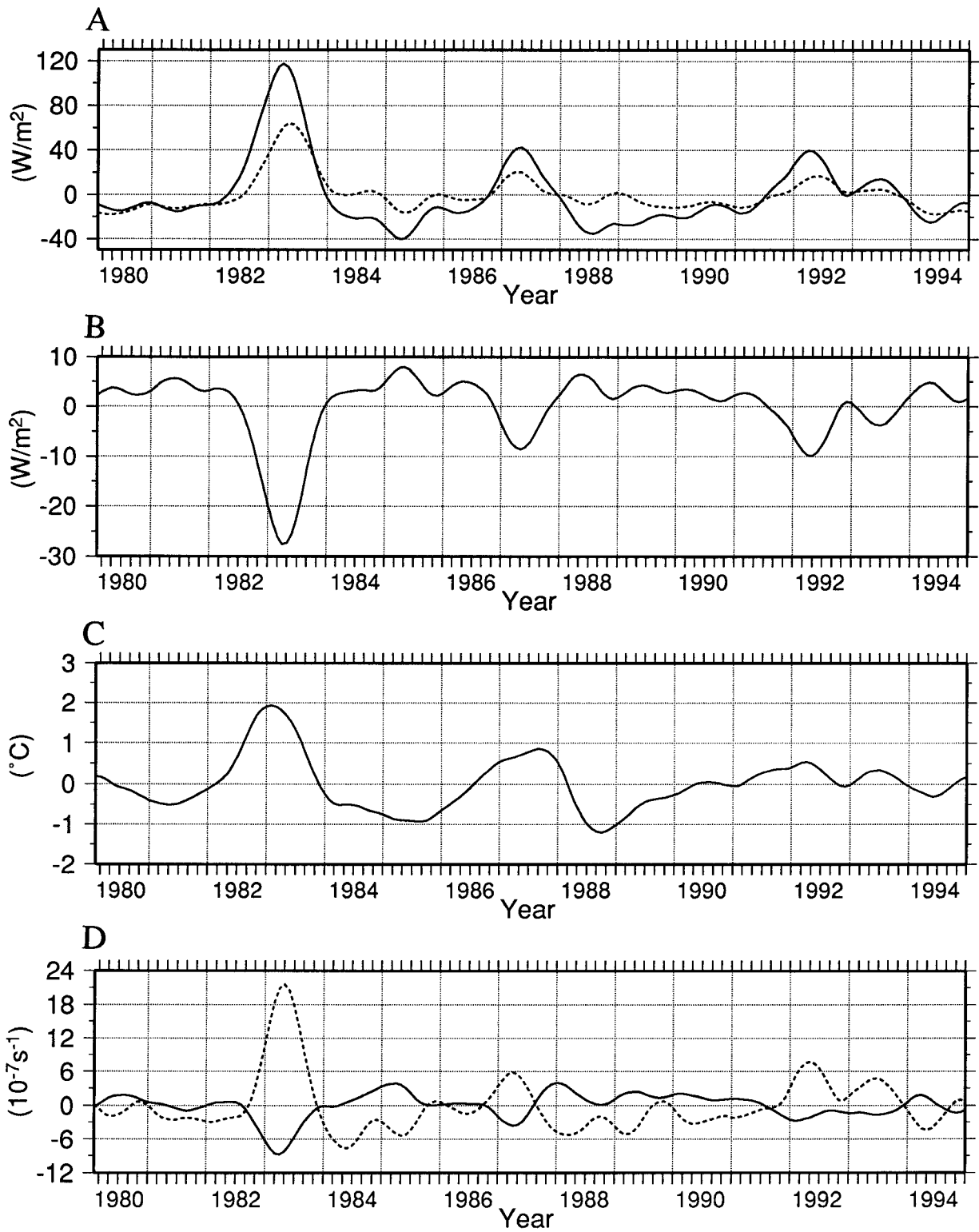


FIG. 7. Time series of the monthly mean anomalies of (a) $\langle Q_1 \rangle$ (solid) and $\langle Q_2 \rangle$ (dashed); (b) OLR; (c) SST; and (d) horizontal divergence at 850 hPa (solid) and 200 hPa (dashed) for the equatorial eastern Pacific Ocean.

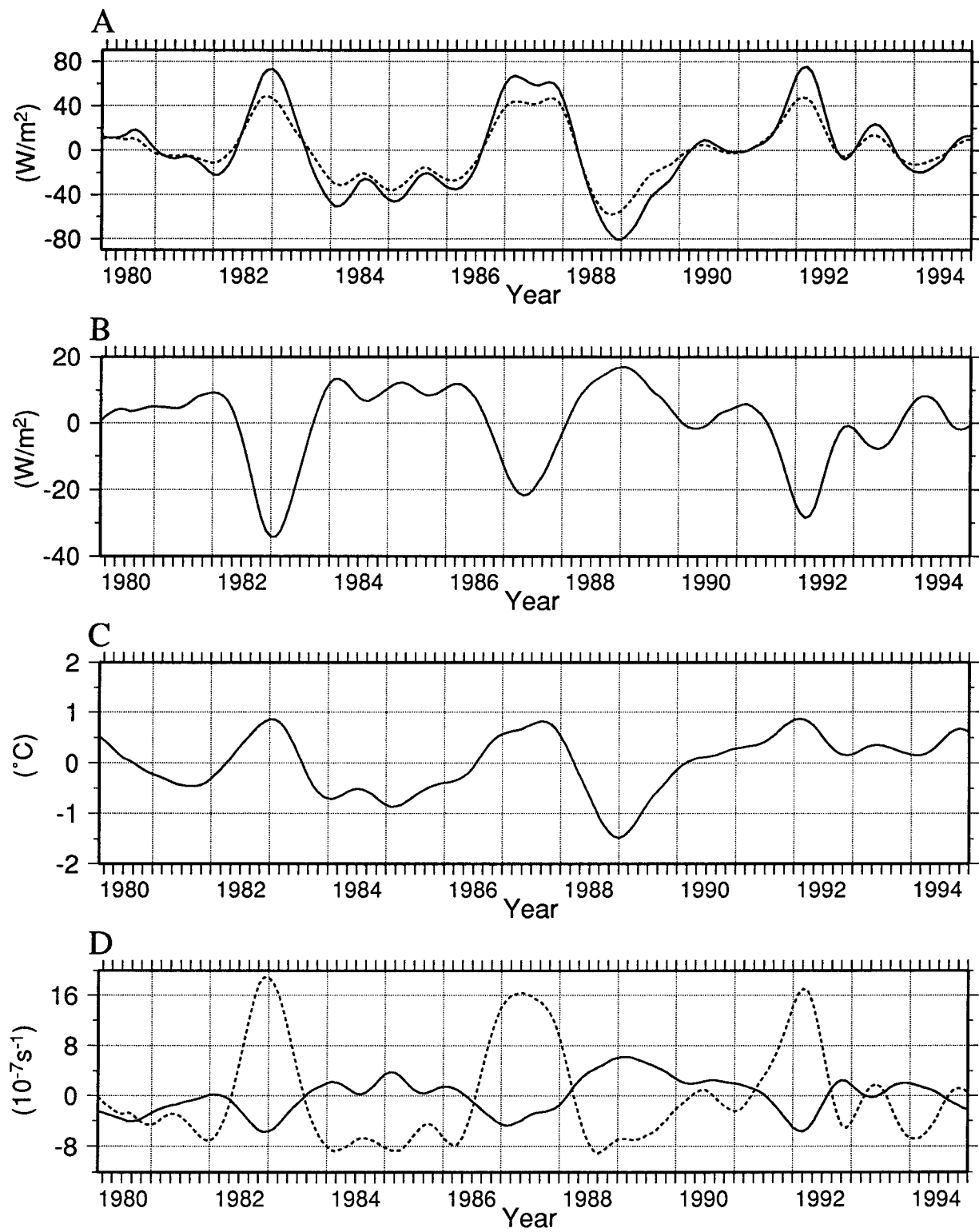


FIG. 8. As in Fig. 7 but for the equatorial central Pacific.

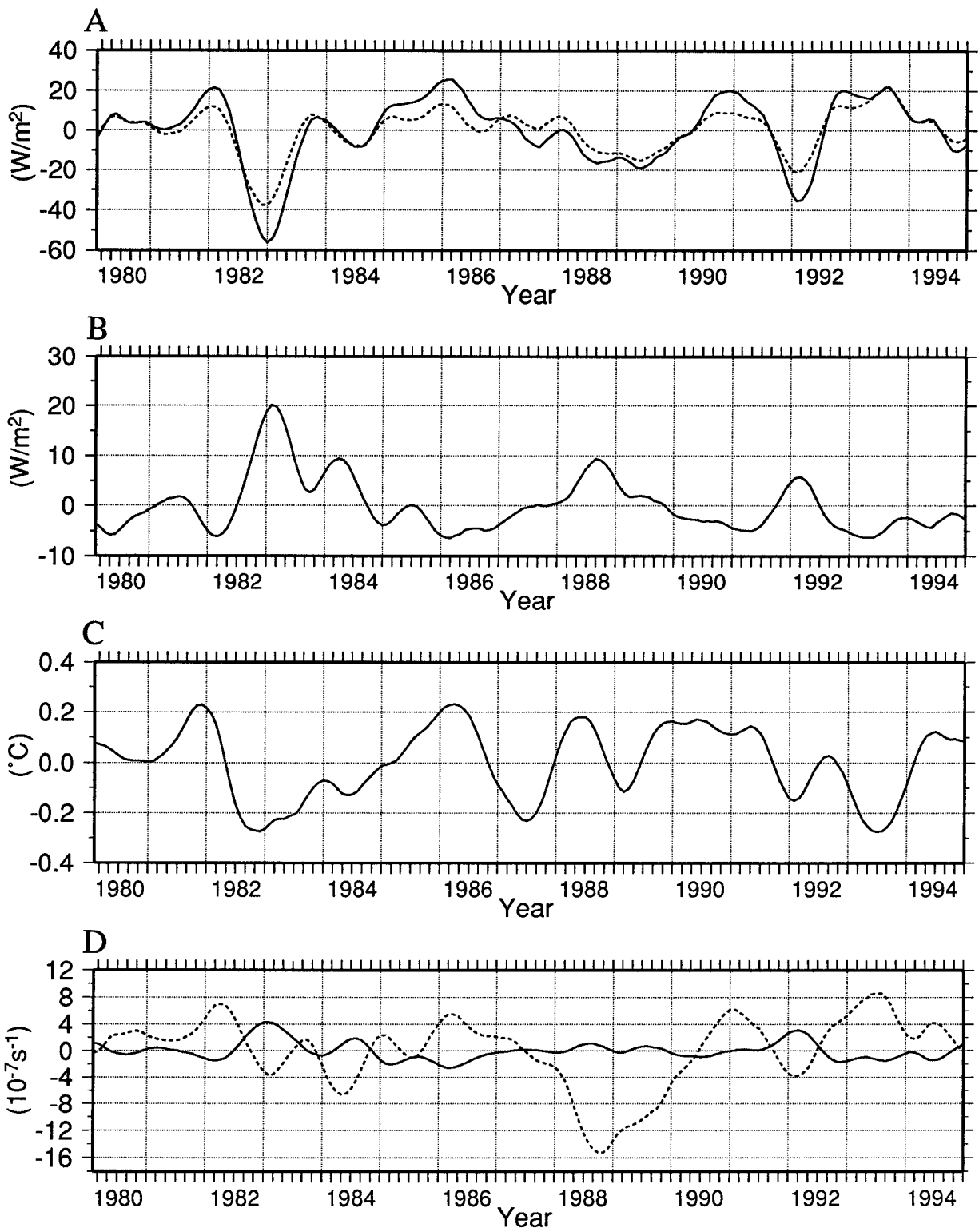


FIG. 9. As in Fig. 7 but for the equatorial western Pacific.

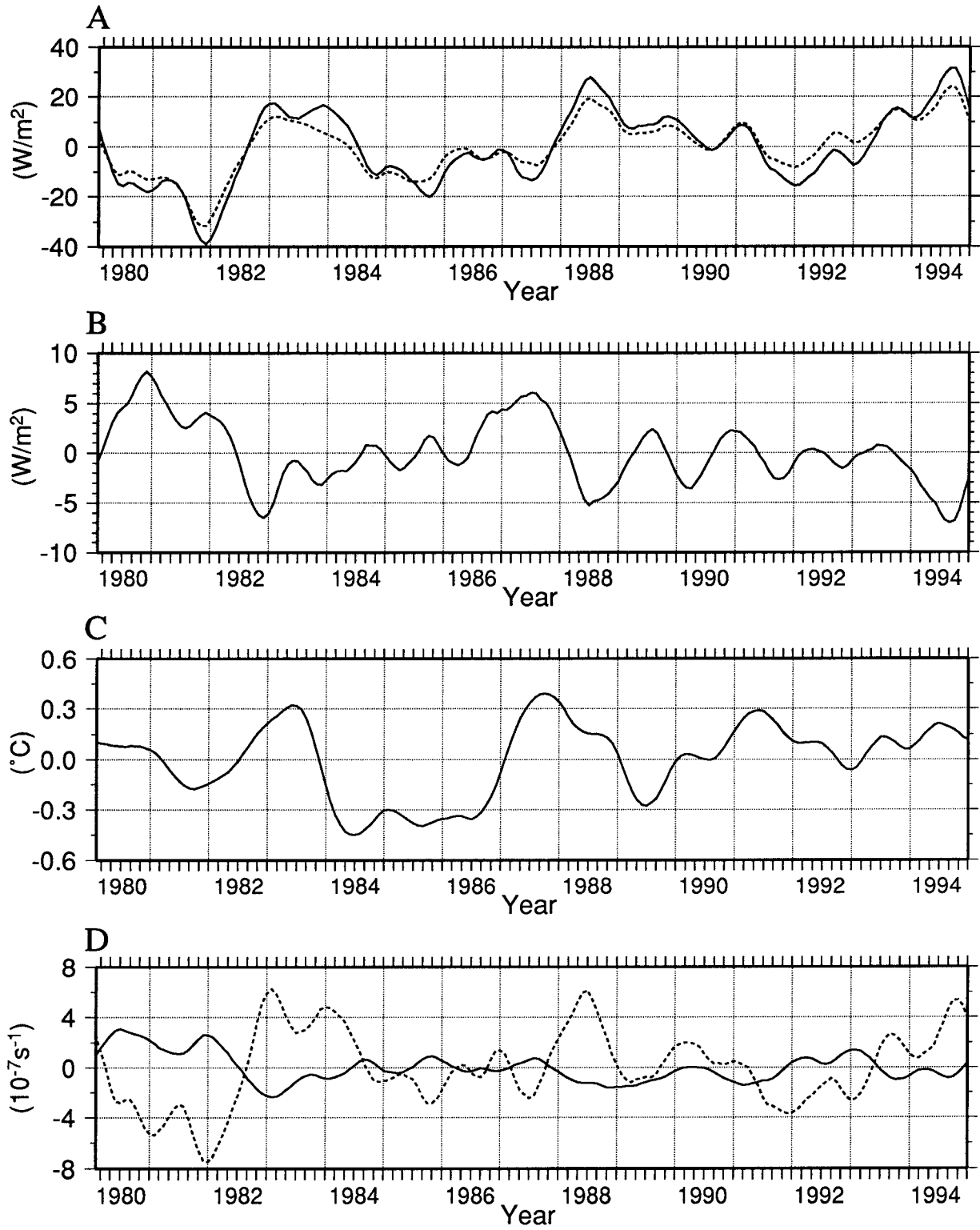


FIG. 10. As in Fig. 7 but for the equatorial Indian Ocean.

TABLE 1. Correlation coefficients between $\langle Q_1 \rangle$ and OLR, SST, and horizontal divergence at 850 hPa (D85) and 200 hPa (D20) for four equatorial oceanic regions.

	OLR	SST	D85	D20
Eastern Pacific	-0.97	0.90	-0.88	0.90
Central Pacific	-0.91	0.92	-0.87	0.92
Western Pacific	-0.83	0.44	-0.89	0.61
Indian Ocean	-0.69	0.34	-0.75	0.90

vergence (D85). The interannual variability of $\langle Q_1 \rangle$ is also highly correlated with horizontal divergence in the upper troposphere (D20) in all sectors except the western Pacific. On the other hand, the positive correlation between $\langle Q_1 \rangle$ and SST is high in the eastern and central Pacific Ocean, but it is low in the western Pacific and Indian Oceans, where the mean SST is above 28°C (Fig. 11).

Overall, there is a strong coupling between $\langle Q_1 \rangle$,

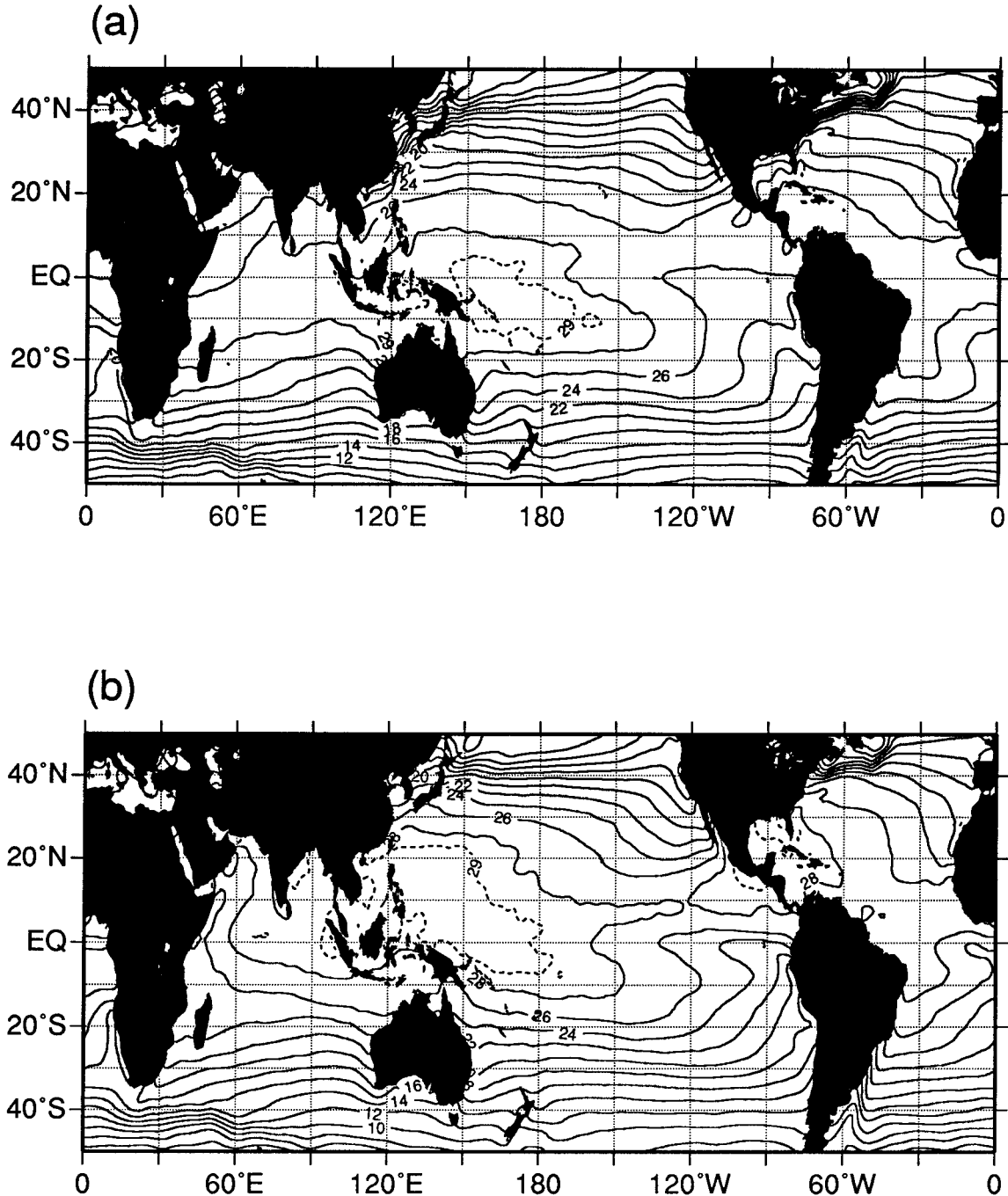


FIG. 11. The 15-yr mean (1980–94) SST (°C): (a) January–March; (b) June–August. The 29°C isotherms are shown by dashed lines.

OLR, and SST in the eastern and central Pacific (also Figs. 7 and 8) showing that the interannual variability of atmospheric heating over these oceans is largely determined by the interannual variability of convective activity, which is in turn controlled by the variability of SST. In contrast, the lower correlations between $\langle Q_1 \rangle$ and SST in the western Pacific and Indian Oceans (also Figs. 9 and 10) suggest that processes other than local SST are at work in controlling the interannual variations in convective activity over these warm oceans.

6. Discussion

In this work, we demonstrated that the simultaneous use of heat and moisture budgets (i.e., analysis of Q_1 and Q_2) applied to the recently released NCEP–NCAR reanalysis can yield a wealth of information on the global heat and moisture source distributions and their seasonal and interannual variability. Analyzing the two quantities Q_1 and Q_2 (introduced in section 2) together, we gain knowledge of not only the amount of atmospheric heating but also the nature of heating (e.g., sensible heat versus latent heat). This method was systematically utilized to interpret the results presented in sections 3 and 4. With the NCEP–NCAR reanalysis program, we can study a long term behavior of atmospheric heat sources and moisture sinks. Our work using the reanalysis (so far 1980–94) has just started and the results on the interannual variability presented in section 5 are of preliminary nature.

The relationship between high SST and tropical convective activity has been a matter of recent intense research (e.g., Ramanathan and Collins 1991; Waliser et al. 1993; Waliser and Graham 1993; Lau et al. 1997). Waliser et al. (1993) showed that at temperatures above about 29.5°C, the amount and intensity of convection tends to decrease with increasing SST. Waliser and Graham (1993) argue that very warm SSTs may only occur under conditions of diminishing convection. In other words, convection acts to decrease and limit SST.

However, our analysis of the interannual variability of Q_1 , OLR, and SST suggest that the variability of convection over the western Pacific warm pool is strongly influenced by the processes other than the local SST effect. This is evident from the phase relationship between the heating anomalies of the western equatorial Pacific and those in the eastern to central equatorial Pacific. The negative anomaly of $\langle Q_1 \rangle$ in the western Pacific during 1982–83 can be understood as a result of suppression of convection influenced by the anomalous large-scale circulation during the ENSO year (e.g., Meehl 1987; Webster 1994; Li and Yanai 1996). Recently, Lau et al. (1997) emphasized the role of large-scale vertical motion in the SST–tropical convection relationship. In the Indian Ocean, both the correlation between $\langle Q_1 \rangle$ and OLR, and that between $\langle Q_1 \rangle$ and SST are low, even though the correlation between $\langle Q_1 \rangle$ and the upper-tropospheric divergence is very high (Table

1). It is well known that SST of the Indian Ocean decreases during the monsoon season. A full explanation of these results requires more work.

In addition to the SST–monsoon relationship (e.g., Rasmusson and Carpenter 1983; Meehl 1987; Yasunari 1990, 1991; Webster and Yang 1992), many authors have studied a statistical relationship between Eurasian snow cover in winter and Indian monsoon rainfall in the following summer (e.g., Hahn and Shukla 1976; Sankar-Rao et al. 1996; Yang 1996). As Shukla (1987) noted, an inverse relationship between Eurasian snow cover and the summer monsoon is not implausible, because large and persistent winter snow cover over Eurasia can delay and weaken the spring and summer heating of the land masses that is necessary for the establishment of the large-scale monsoon flow. Recently, a number of numerical experiments have been carried out to test the sensitivity of the global climate system to the variability of the Eurasian snow cover (Barnett et al. 1989; Yasunari et al. 1991; Vernekar et al. 1995; Douville and Royer 1996; Ose 1996). Their results suggest potential importance of land processes in global climate dynamics affecting the ENSO events. Systematic investigations of interannual variability of heat sources, SST, and snow cover will add a new knowledge to the understanding of ENSO–monsoon interaction.

Yanai and Li (1994b) showed that there are three distinct peaks near 3–6 and 2–2.5 yr and near 15 months in the power spectra of the monsoon intensity index (Webster and Yang 1992), the equatorial SST, and the Eurasian snow cover. The quasi-biennial appearance of tropical variables such as sea level pressure, SST, and precipitation has been known by many studies (e.g., Trenberth 1975; Trenberth and Shea 1987; Lau and Sheu 1988; Rasmusson et al. 1990; Jiang et al. 1996; Tomita and Yasunari 1996). The biennial tendency of the NH snow cover has been pointed out by Iwasaki (1991). Is the biennial tendency of the snow cover a response to the biennial pulse of large-scale circulation caused by the fluctuation of SST? These are interesting questions for future research.

The NCEP–NCAR reanalysis, however, is not free from defects. We note from the comparisons of $\langle Q_1 \rangle$ and $\langle Q_2 \rangle$, presented in Figs. 1–4, that the ITCZ and SPCZ are less clearly defined in the $\langle Q_2 \rangle$ field. This problem has been documented independently by Trenberth and Guillemot (1996). From an extensive evaluation of the precipitable water and hydrological cycle, they concluded that the NCEP–NCAR moisture fields have negative biases in the Tropics. With the recently released ECMWF reanalysis, the global heat and moisture budgets and their consistency with the relations (10) and (11) need to be quantitatively examined. We have started intercomparisons of the $\langle Q_1 \rangle$ and $\langle Q_2 \rangle$ fields obtained using the NCEP–NCAR reanalysis and those using the ECMWF reanalysis based on 4 samplings a day (0000, 0600, 1200, and 1800 UTC).

Acknowledgments. The authors thank Chengfeng Li who participated in the early phase of this research. Two anonymous reviewers offered useful comments on the first version of this paper. They acknowledge Baode Chen for his unflinching help in various aspects of this work. This work was supported by the National Science Foundation under Grant ATM-9500338 and by the National Oceanic and Atmospheric Administration under Grant NA56GP0203. The computations were performed at computing facilities at NCAR/Scientific Computing Division and the Department of Atmospheric Sciences at University of California, Los Angeles.

REFERENCES

- Ackerman, S. A., and S. K. Cox, 1987: Radiative energy budget estimates for the 1979 southwest summer monsoon. *J. Atmos. Sci.*, **44**, 3052–3078.
- Barnett, T. P., L. Dümenil, U. Schlese, E. Roeckner, and M. Latif, 1989: The effect of Eurasian snow cover on regional and global climate variations. *J. Atmos. Sci.*, **46**, 661–685.
- Christy, J. R., 1991: Diabatic heating rate estimates from European Centre for Medium-Range Weather Forecasts analyses. *J. Geophys. Res.*, **96**, 5123–5135.
- Dopplack, T. G., 1979: Radiative heating of the global atmosphere: Corrigendum. *J. Atmos. Sci.*, **36**, 1812–1817.
- Douglas, M. W., R. A. Maddox, and K. Howard, 1993: The Mexican monsoon. *J. Climate*, **6**, 1665–1677.
- Douville, D., and J.-F. Royer, 1996: Sensitivity of the Asian summer monsoon to an anomalous Eurasian snow cover within the Meteor-France GCM. *Climate Dyn.*, **12**, 449–466.
- Hahn, D. G., and J. Shukla, 1976: An apparent relationship between Eurasian snow cover and Indian monsoon rainfall. *J. Atmos. Sci.*, **33**, 2461–2462.
- He, H., J. W. McGinnis, Z. Song, and M. Yanai, 1987: Onset of the Asian monsoon in 1979 and the effect of the Tibetan Plateau. *Mon. Wea. Rev.*, **115**, 1966–1995.
- Hoskins, B. J., H. H. Hsu, I. N. James, M. Masutani, P. D. Sardeshmukh, and G. H. White, 1989: Diagnostics of the global atmospheric circulation based on ECMWF analyses 1979–1989. World Climate Research Programme-27, WMO/TD-326, 217 pp.
- Iwasaki, T., 1991: Year-to-year variation of snow cover area in the Northern Hemisphere. *J. Meteor. Soc. Japan*, **69**, 209–217.
- Jiang, N., J. D. Neelin, and M. Ghil, 1995: Quasi-quadrennial and quasi-biennial variability in equatorial Pacific. *Climate Dyn.*, **12**, 101–112.
- Johnson, D. R., M. Yanai, and T. K. Schaack, 1987: Global and regional distributions of atmospheric heat sources and sinks during the GWE. *Monsoon Meteorology*, C. P. Chang and T. N. Krishnamurti, Eds., Oxford University Press, 271–297.
- Joseph, P. V., J. K. Eischeid, and R. J. Pyle, 1994: Interannual variability of the onset of the Indian summer monsoon and its association with atmospheric features, El Niño, and sea surface temperature anomalies. *J. Climate*, **7**, 81–105.
- Kalnay, E., and Coauthors, 1996: The NCEP/NCAR 40-year reanalysis project. *Bull. Amer. Meteor. Soc.*, **77**, 437–471.
- Krishnamurti, T. N., H. S. Bedi, and M. Subramaniam, 1989: The summer monsoon of 1987. *J. Climate*, **2**, 321–340.
- , —, and —, 1990: The summer monsoon of 1988. *Meteor. Atmos. Phys.*, **42**, 19–37.
- Lau, K. M., and P. J. Sheu, 1988: Annual cycle, quasi-biennial oscillation, and Southern Oscillation. *J. Geophys. Res.*, **93**, 10975–10988.
- , H.-T. Wu, and S. Bony, 1997: The role of large-scale atmospheric circulation in the relationship between tropical convection and sea surface temperature. *J. Climate*, **10**, 381–392.
- Li, C., and M. Yanai, 1996: The onset and interannual variability of the Asian summer monsoon in relation to land–sea thermal contrast. *J. Climate*, **9**, 358–375.
- Luo, H., and M. Yanai, 1984: The large-scale circulation and heat sources over the Tibetan Plateau and surrounding areas during the early summer of 1979. Part II: Heat and moisture budgets. *Mon. Wea. Rev.*, **112**, 966–989.
- Meehl, G. A., 1987: The annual cycle and interannual variability in the tropical Pacific and Indian Ocean regions. *Mon. Wea. Rev.*, **115**, 27–50.
- Mohanty, U. C., S. K. Dube, and M. P. Singh, 1983: A study of heat and moisture budgets over the Arabian Sea and their role in the onset and maintenance of summer monsoons. *J. Meteor. Soc. Japan*, **61**, 208–221.
- Nitta, T., 1977: Response of cumulus updraft and downdraft to GATE A/B-scale motion systems. *J. Atmos. Sci.*, **34**, 1163–1186.
- , 1983: Observational study of heat sources over the eastern Tibetan Plateau during the summer monsoon. *J. Meteor. Soc. Japan*, **61**, 590–605.
- Ose, T., 1996: The comparison of the simulated response to the regional snow mass anomalies over Tibet, Eastern Europe, and Siberia. *J. Meteor. Soc. Japan*, **74**, 845–866.
- Philander, S. G., 1990: *El Niño, La Niña, and the Southern Oscillation*. Academic Press, 293 pp.
- Ramanathan, V., and W. Collins, 1991: Thermodynamic regulation of ocean warming by cirrus clouds deduced from observations of the 1987 El Niño. *Nature*, **351**, 27–32.
- Rao, G. V., W. R. Schaub Jr., and J. Puetz, 1981: Evaporation and precipitation over the Arabian Sea during several monsoon seasons. *Mon. Wea. Rev.*, **109**, 364–370.
- Rasmusson, E. M., and T. H. Carpenter, 1982: Variations in tropical sea surface temperature and surface wind fields associated with the Southern Oscillation/El Niño. *Mon. Wea. Rev.*, **110**, 354–384.
- , and —, 1983: The relationship between the eastern equatorial Pacific sea surface temperatures and rainfall over India and Sri Lanka. *Mon. Wea. Rev.*, **111**, 517–528.
- , X. Wang, and C. F. Ropelewski, 1990: The biennial component of ENSO variability. *J. Mar. Syst.*, **1**, 71–96.
- Ropelewski, C. F., and M. S. Halpert, 1987: Global- and regional-scale precipitation patterns associated with the El Niño/Southern Oscillation. *Mon. Wea. Rev.*, **115**, 1606–1626.
- , and —, 1989: Precipitation patterns associated with the high index phase of the Southern Oscillation. *J. Climate*, **2**, 268–284.
- Sankar-Rao, M., K. M. Lau, and S. Yang, 1996: On the relationship between Eurasian snow cover and the Asian summer monsoon. *Int. J. Climatol.*, **16**, 605–616.
- Schaack, T. K., and D. R. Johnson, 1994: January and July global distributions of atmospheric heating for 1986, 1987, and 1988. *J. Climate*, **7**, 1270–1285.
- , —, and M.-Y. Wei, 1990: The three-dimensional distribution of atmospheric heating during the GWE. *Tellus*, **42A**, 305–327.
- Shukla, J., 1987: Interannual variability of monsoons. *Monsoons*, J. S. Fein and P. L. Stephens, Eds., John Wiley and Sons, 399–463.
- Thompson, R. M., Jr., S. W. Payne, E. E. Recker, and R. J. Reed, 1979: Structure and properties of synoptic-scale wave disturbances in the intertropical convergence zone of the eastern Atlantic. *J. Atmos. Sci.*, **36**, 53–72.
- Tomita, T., and T. Yasunari, 1996: Role of the northeast winter monsoon on the biennial oscillation of the ENSO/monsoon system. *J. Meteor. Soc. Japan*, **74**, 399–413.
- Trenberth, K. E., 1975: A quasi-biennial standing wave in the Southern Hemisphere and interrelations with sea surface temperature. *Quart. J. Roy. Meteor. Soc.*, **101**, 55–74.
- , 1984: Signal versus noise in the Southern Oscillation. *Mon. Wea. Rev.*, **112**, 326–332.
- , 1992: Global analyses from ECMWF and atlas of 1000 to 10 mb circulation statistics. NCAR Tech. Note NCAR/TN-373+STR, 191 pp.

- , and D. J. Shea, 1987: On the evolution of the Southern Oscillation. *Mon. Wea. Rev.*, **115**, 3078–3096.
- , and J. G. Olson, 1988: ECMWF global analyses 1976–86: Circulation statistics and data evaluation. NCAR Tech. Note NCAR/TN-300+STR, 94 pp. plus 12 fiche.
- , and A. Solomon, 1994: The global heat balance: Heat transports in the atmosphere and ocean. *Climate Dyn.*, **10**, 107–134.
- , and C. J. Guillemot, 1996: Evaluation of the atmospheric moisture and hydrological cycle in the NCEP reanalyse. NCAR Tech. Note TN-430+STR, 308 pp.
- Vernekar, A. D., J. Zhou, and J. Shukla, 1995: The effect of Eurasian snow cover on the Indian monsoon. *J. Climate*, **8**, 248–266.
- Waliser, D. E., and N. E. Graham, 1993: Convective cloud systems and warm-pool sea surface temperatures: Coupled interactions and self-regulation. *J. Geophys. Res.*, **98**, 12 881–12 893.
- , —, and C. Gautier, 1993: Comparison of the highly reflective cloud and outgoing longwave radiation datasets for use in estimating tropical deep convection. *J. Climate*, **6**, 331–353.
- Webster, P. J., 1994: The role of hydrological processes in ocean–atmosphere interactions. *Rev. Geophys.*, **32**, 427–476.
- , and S. Yang, 1992: Monsoon and ENSO: Selectively interactive systems. *Quart. J. Roy. Meteor. Soc.*, **118**, 877–926.
- Wei, M.-Y., D. R. Johnson, and R. D. Townsend, 1983: Seasonal distributions of diabatic heating during the First GARP Global Experiment. *Tellus*, **35A**, 241–255.
- Yanai, M., and R. H. Johnson, 1993: Impacts of cumulus convection on thermodynamic fields. *Representation of Cumulus Convection in Numerical Models of the Atmosphere*, Meteor. Monogr., No. 46, Amer. Meteor. Soc., 39–62.
- , and C. Li, 1994a: Mechanism of heating and the boundary layer over the Tibetan Plateau. *Mon. Wea. Rev.*, **122**, 305–323.
- , and —, 1994b: Interannual variability of the Asian summer monsoon and its relationship with ENSO, Eurasian snow cover, and heating. *Proc. Int. Conf. on Monsoon Variability and Prediction*, Trieste, Italy, World Meteorological Organization, 27–34.
- , and —, 1996: Seasonal and interannual variability of atmospheric heating. Preprints, *Eighth Conf. on Air–Sea Interaction and Symposium on GOALS*, Atlanta, GA, Amer. Meteor. Soc., 102–106.
- , S. Esbensen, and J.-H. Chu, 1973: Determination of bulk properties of tropical cloud clusters from large-scale heat and moisture budgets. *J. Atmos. Sci.*, **30**, 611–627.
- , C. Li, and Z. Song, 1992: Seasonal heating of the Tibetan Plateau and its effects on the evolution of the Asian summer monsoon. *J. Meteor. Soc. Japan*, **70**, 319–351.
- Yang, S., 1996: ENSO–snow–monsoon associations and seasonal–interannual predictions. *Int. J. Climatol.*, **16**, 125–134.
- Yasunari, T., 1990: Impact of Indian monsoon on the coupled atmosphere/ocean system in the tropical Pacific. *Meteor. Atmos. Phys.*, **44**, 29–41.
- , 1991: The monsoon year—A new concept of the climatic year in the Tropics. *Bull. Amer. Meteor. Soc.*, **72**, 1331–1338.
- , A. Kitoh, and T. Tokioka, 1991: Local and remote responses to excessive snow mass over Eurasia appearing in the northern spring and summer climate—A study with the MRI-GCM. *J. Meteor. Soc. Japan*, **69**, 473–487.